Cell and Tissue Research (2019) 378:97–111
https://doi.org/10.1007/s00441-019-03023-9

REGULAR ARTICLE

# Mouse model to study pulmonary intravascular macrophage recruitment and lung inflammation in acute necrotizing pancreatitis

Vanessa Vrolyk[1] · David Schneberger[1] · Khanh Le[1] · Bruce K. Wobeser[2] · Baljit Singh[1,3]

Received: 21 August 2018 / Accepted: 27 March 2019 / Published online: 29 April 2019


## Abstract

Patients suffering from severe acute pancreatitis (AP) can develop acute lung injury (ALI) with poor outcomes and the mechanisms involved remain incompletely understood. Pulmonary intravascular macrophages (PIMs), which are credited as promoters of ALI, are not constitutively present in humans and rodents; however, there is evidence of PIM recruitment in rodents during some pathological conditions, such as hepatic diseases. Therefore, this study assesses PIM recruitment in the lungs of a mouse model of acute necrotizing pancreatitis (ANP) induced with L-arginine monohydrochloride. Mice were euthanized after 24 h, 72 h and 120 h. Control mice received sham injections of saline. Pancreatic histopathological grading and plasma amylase were used to confirm the development of ANP in L-arginine-treated mice. Histopathological grading of lungs from the ANP mice at 72 h showed increased mononuclear phagocytes in alveolar septa, compared to that from the controls. Lungs from the ANP mice also showed increased numbers of CD68-immunopositive alveolar septal macrophages, suggestive of PIM recruitment, compared to those from the controls. Lungs from the ANP mice showed increased expression of IL-6, IL-10, monocyte chemoattractant protein 1 (MCP-1) and von Willebrand factor compared to those from the controls. The recruitment of CD68-positive septal macrophages was not observed in MCP-1 knockout mice with ANP at 72 h when compared to C57BL/6 wild-type mice. Taken together, we developed a mouse model of PIM recruitment dependent on MCP-1 that allows us to explore their roles in ANP-associated ALI.

**Keywords** Pulmonary intravascular macrophage · Pancreatitis · CD68 · Mouse · vWF

Severe acute pancreatitis (AP) is a common gastrointestinal cause of emergency admissions in human patients with a globally increasing annual incidence varying from 13 to 45 episodes/100,000/year (Pintado et al. 2016; Spanier et al. 2013). While mild pancreatitis results in a complete recovery in most patients, severe acute pancreatitis, including acute necrotizing pancreatitis (ANP), is associated with significant morbidity and high mortality rates varying from 18% in people aged between 50 and 74 years old to 85% in people older than 75 years old (Spanier et al. 2013). This condition is commonly accompanied by a systemic inflammatory response syndrome and approximately 77–100% of patients admitted to the intensive care unit for severe AP develop a multiple organ dysfunction syndrome (Pintado et al. 2016). Among all systemic complications reported in people with severe AP, respiratory complications have the highest incidence ranging from 57 to 62% of patients. Furthermore, the development of an acute respiratory distress syndrome is commonly reported as the main cause of death associated with this disease (Pintado et al. 2016). In addition, 78–90% of patients diagnosed with severe AP required mechanical ventilation, illustrating the high morbidity (Pintado et al. 2016). The high mortality rates and the lack of efficient treatments for patients with severe AP–associated pulmonary complications result from our poor understanding of the pathophysiology, leading to the

**Electronic supplementary material** The online version of this article (https://doi.org/10.1007/s00441-019-03023-9) contains supplementary material, which is available to authorized users.

✉ Baljit Singh
baljit.singh1@ucalgary.ca

[1] Department of Veterinary Biomedical Sciences, Western College of Veterinary Medicine, University of Saskatchewan, 52 Campus Drive, Saskatoon, Saskatchewan S7N 5B4, Canada

[2] Department of Veterinary Pathology, Western College of Veterinary Medicine, University of Saskatchewan, 52 Campus Drive, Saskatoon, Saskatchewan S7N 5B4, Canada

[3] Faculty of Veterinary Medicine, University of Calgary, Calgary, AB T2N 4Z6, Canada

development of an acute respiratory distress syndrome in this condition.

In the past decades, numerous studies using rodent models of severe AP have been conducted to investigate the mechanisms involved in the development of acute lung injury or acute respiratory distress syndrome, during severe AP. The development of pulmonary complications related with severe AP is considered multifactorial and involves the release into the blood circulation of pancreas-specific proteins (Tahamont et al. 1982; Tsukahara et al. 1999), the activation of Kupffer cells (Hoyos et al. 2005) and peritoneal macrophages (Mikami et al. 2002) and gut barrier dysfunction (Ammori 2003). In rodent models of severe AP, lung injury is characterized by the early recruitment of neutrophils into the alveolar septa and the alveoli (Tahamont et al. 1982), vascular injury leading to lung edema or hemorrhage, the activation of alveolar macrophages in a pro-inflammatory phenotype (Gea-Sorli et al. 2011), as well as the production of various pro-inflammatory cytokines and nitric oxide (Gea-Sorli et al. 2011; Tsukahara et al. 1999). Alveolar macrophages have been widely targeted as crucial players in the development of pulmonary complications secondary to severe AP (Gea-Sorli et al. 2011; Zhao et al. 2017). There, however, are no data on the recruitment and function of another type of macrophage, pulmonary intravascular macrophages (PIMs), in AP-related lung injury.

PIMs are highly phagocytic large cells (20–80 μm diameter) with characteristics of mature macrophages and are attached to the endothelium of septal capillaries in the lung (Warner et al. 1986). Some species have constitutive PIMs such as in the orders *Artiodactyla* (cattle, sheep, goats and pigs) (Brain et al. 1999; Warner et al. 1986), *Perissodactyla* (horses) (Atwal et al. 1992) and *Odontoceti* cetacean (toothed whales) (Kawashima et al. 2004) and in some strains of domestic cat (Molina and Brain 2007), whereas other species including rodents and dogs do not have constitutive PIMs (Gill et al. 2008; Schneberger et al. 2011; Vrolyk et al. 2016). Nevertheless, PIMs were shown to be recruited (referred to as induced PIMs) in rats suffering from various systemic pathological conditions including liver diseases and *Escherichia coli* sepsis (Gill et al. 2008; Singh et al. 1998). The ultrastructural reports on human lungs suggest that healthy individuals have rare constitutive PIMs (Dehring and Wismar 1989). However, there has been indirect evidence suggesting the recruitment of PIMs in people suffering from liver dysfunction, which resembles the observations made in other species devoid of constitutive PIMs (Klingensmith 3rd and Ryerson 1973; Shih et al. 1986).

In various species with different systemic conditions, constitutive or induced PIMs are considered to be pro-inflammatory and express microbial receptors such as TLR4, TLR2 and TLR9 (Gill et al. 2008; Schneberger et al. 2009; Singh Suri et al. 2006); produce pro-inflammatory cytokines (IL-1, TNF-α); and can recruit IL-8–containing platelets (Gill et al. 2008; Singh et al. 2004). Furthermore, it has been suggested that both constitutive and induced PIMs enhance the host susceptibility to develop an exacerbated lung inflammatory response following subsequent microbial challenges and their depletion (Aharonson-Raz and Singh 2010; Gill et al. 2008). The observation that depletion of induced PIMs in bile duct–ligated rats inhibits endotoxin-induced lung inflammation further stresses the pro-inflammatory role of induced PIMs (Gill et al. 2008). Nevertheless, there are no data on the recruitment/induction of PIMs in ANP.

Recently, we reported the first evidence on the occurrence of PIMs in dogs that died of spontaneous ANP (Vrolyk et al. 2016). Similar to humans, dogs do not possess constitutive PIMs but present respiratory clinical signs during ANP. To develop a mouse model to study the role of induced PIMs in ANP, we tested the hypothesis that PIMs are recruited in a mouse model of L-arginine–induced ANP and that PIM recruitment is dependent on the monocyte chemoattractant protein 1 (MCP-1).

## Material and methods

### Reagents

L-arginine monohydrochloride (cat no. 11039-100G) and endotoxin-free saline (S8776) used to prepare the L-arginine solution were purchased from Sigma-Aldrich, Oakville, Ontario, Canada and cetyltrimethylammonium chloride (CTAC), 3′,5,5′-tetramethylbenzidine hydrochloride (TMB) and myeloperoxidase (MPO) from human leukocytes (M6908-5U) were used in the MPO assay. The DC Protein Assay kit and the Bio-Plex Multiplex immunoassay were purchased from Bio-Rad, Mississauga, Ontario, Canada.

### Animals

Six-to-eight-week-old male C57BL/6 (19–27 g) mice ($N = 30$) were purchased from Charles River Laboratories (Montréal, Québec, Canada) and 6-to-8-week-old male MCP-1 (B6.129S4-Ccl2tm1Rol/J) knockout mice ($N = 10$) were purchased from Jackson Labs (Bar Harbor, ME, USA). Mice were housed individually in the Animal Care Unit of the Western College of Veterinary Medicine of the University of Saskatchewan in standard shoebox cages in a controlled room with an ambient temperature of 23 °C ± 2 °C and a 12-h light-dark cycle. They were fed a standard laboratory chow and had water ad libitum. Mice were euthanized by exsanguination through intracardiac puncture under general anesthesia achieved by an intraperitoneal injection of a ketamine/xylazine mix (10:1) at a dose of 1–2% of body weight. All experiments were performed according to protocols approved

by the University of Saskatchewan Committee on Animal Care Assurance.

## L-Arginine–induced ANP mouse model protocol

A sterile L-arginine monohydrochloride 9% solution in endotoxin-free saline at pH 7.0 was prepared fresh on the day of ANP induction. The L-arginine solution was filtered with a syringe filter (0.2 μm pore, 25 mm diameter) into a pharmaceutical sealed glass vial to ensure sterility. The L-arginine ANP induction protocol used in this study followed the method described by Dawra et al. (2007) with some modifications; two intraperitoneal injections of the L-arginine 9% solution were administered, 1 h apart, at a dose of 4.5 g/kg using a 27-G needle and a 1-ml syringe. Control mice received sham injections of physiological sterile saline. All mice, including control mice, were administered two injections of 1.5 ml to 2 ml of sterile physiological saline subcutaneously to prevent dehydration during the initial morbidity phase associated with the injections of the L-arginine solution; the first saline injection was administered at the time of the last injection of L-arginine while the second saline injection was administered 3 h afterward. This L-arginine ANP induction protocol was followed for both the C57BL/6 wild-type mice (experiment 1) and the MCP-1 knockout mice (experiment 2).

## Experimental design

### Experiment 1

C57BL/6 wild-type mice were randomly divided into the following groups based on the time of euthanasia after the induction of ANP: 24 h ANP ($n = 7$), 72 h ANP ($n = 7$) and 120 h ANP ($n = 7$). Three control mice were included in each timepoint group.

### Experiment 2

Since the 72-h timepoint in experiment 1 was associated with the most significant pathological changes in the lungs of mice with ANP, including recruitment of alveolar septal mononuclear phagocytes, this timepoint was selected to perform experiment 2. MCP-1 knockout mice were randomly divided into a L-arginine–induced ANP group ($n = 5$) and a control group ($n = 5$). All mice in experiment 2 were euthanized 72 h after the induction of ANP.

## Histopathology and grading of lesions

The left lung and the pancreas were collected from all mice, including control and ANP mice from both experiments, for fixation in 4% paraformaldehyde followed by embedding in paraffin. Briefly, the right bronchus was ligated and the left lung was instilled with approximately 1 ml of 4% paraformaldehyde under a 20 cm water pressure while the trachea was ligated to prevent backflow. The instilled left lung and the pancreas were removed and fixed in 4% paraformaldehyde overnight at 4 °C (between 16 and 20 h) for paraffin embedding and the right lung was removed and kept in liquid nitrogen for the MPO assay and the Bio-Plex Multiplex immunoassay.

The pancreatic and the lung histological sections from all ANP and control mice (experiments 1 and 2) were graded by a specialist veterinary pathologist in a blinded manner using the criteria shown in Tables 1 and 2.

## Collection of bronchoalveolar lavage

Bronchoalveolar lavage (BAL) was performed on the left lung prior to its fixation with 4% paraformaldehyde. After thoracotomy and the ligation of the right primary bronchus, a small incision was made in the trachea to insert a small flexible cannula up to the tracheal bifurcation. Three lavages were performed on the lung from each mouse using each time 0.5 ml of cold sterile phosphate-buffered saline (PBS) (pH 7.4) in a 1-ml syringe. White blood cell counts and cytospins for differential counts were performed quickly after the BAL fluid collection. The remaining BAL supernatant was kept at − 80 °C for further analysis.

## Immunohistochemistry

Immunohistochemical labeling was performed on lung sections from all mice with ANP and control mice from both experiments, as previously described (Singh Suri et al. 2006). Briefly, sections were deparaffinized, rehydrated in descending concentrations of ethanol and incubated with 0.5% $H_2O_2$ in methanol for 20 min to quench the endogenous peroxidase activity. Antigen retrieval was performed using pepsin (2 mg/ml in 0.01 N HCl) for 1 h at room temperature, after which blocking was done with bovine serum albumin (BSA) (1% in PBS) for 30 min at room temperature. Slides were incubated overnight (16 h) at 4 °C with the following primary antibodies: polyclonal rabbit anti-human CD68 (Sc-9139) (1:25; Santa Cruz Biotechnology, Dallas, TX, USA) and polyclonal rabbit anti-human von Willebrand factor (vWF) antibody (P0448) (1:400; DAKO, Ottawa, Canada). Then, sections were incubated for 30 min at room temperature with the appropriate horseradish peroxidase (HRP)–conjugated secondary antibody (1:100; except against vWF [1:300], all from DAKO). Color development was performed using a commercial kit (Vector Laboratories, Ontario, Canada) followed by counterstaining with methyl green to delineate the nuclei.

Immunohistochemical controls consisted of omission of the primary antibody for all different secondary antibodies used and incubation with the appropriate isotype-matched antibodies. In addition, labeling with vWF was used as a positive

**Table 1** Pancreatic histopathology score: sum of necrosis, edema and inflammatory cell infiltrate scores

| | Pancreatic histopathological assessment scores | | | | | |
|---|---|---|---|---|---|---|
| | 0 | 1 | 2 | 3 | 4 | 5 |
| Necrosis | Absent | Loss of zymogen granules | < 10% of the pancreatic parenchyma | 10% to 25% of the pancreatic parenchyma | 25% to 50% of the pancreatic parenchyma | Diffuse pancreatic necrosis; > 50% of the pancreatic parenchyma |
| Edema | Absent | Focally increased space between lobules | Diffusely increased space between lobules | Pancreatic acini disrupted and separated | | |
| Inflammatory cell infiltrate | Absent | Rare inflammatory cell or only around ductal margins | In the pancreatic parenchyma (< 50% of the lobules) | In the pancreatic parenchyma (> 50% of the lobules) | | |

**Table 2** Lung histopathology score: sum of edema and inflammatory cell

| | Lung histopathological assessment scores | | | |
|---|---|---|---|---|
| | 0 | 1 | 2 | 3 |
| Edema | Absent | Mild | Moderate | Severe |
| Inflammatory cell infiltrate | Absent | Mild | Moderate | Severe |

control. Both negative controls resulted in the absence of labeling, whereas vWF labeled the vascular endothelium but not the airway epithelium.

## Quantification of cells labeled with CD68 antibody

A two-dimensional (2D)–modified morphological analysis was used to count the number of positively labeled CD68 cells present in alveolar septa; photographs of 10 random fields of view at × 400 magnification were captured using a light microscope (Olympus BX53; Olympus, Richmond Hill, Ontario, Canada) and a digital camera (Olympus DP21) for each of the ANP and control mice from both experiments. Fields of view including large blood vessels or airways were ignored, continuing to the following field of view in a constant predetermined pattern. Then, using ImageJ software (1.49v Rasband, W.S.; ImageJ, National Institutes of Health, Bethesda, MD, USA), a 13 × 13 intersect-counting grid was superimposed onto each microscopically captured field of view. For every field of view, the number of grid intersects overlaying CD68-positive mononuclear phagocyte profiles present in alveolar septa was recorded. This was performed for each of the control and ANP mice. To normalize the potential variations in lung morphology between mice, the number of grid intersects overlaying alveolar septa in each captured image was simultaneously recorded. The total numbers of grid intersects overlaying CD68-positive mononuclear phagocyte profiles and alveolar septa were calculated using all 10 fields of view per animal. Then, for each of the control and ANP mice, a ratio was calculated dividing the total number of grid intersects overlaying CD68-positive mononuclear phagocyte profiles by the total number of grid intersects overlaying alveolar septa, thus controlling for the variability of lung morphology alterations between cases.

## Myeloperoxidase activity in the lungs of mice

The MPO assay was performed on lung tissues from control and ANP mice from experiment 1 only. Briefly, the homogenized lung samples were centrifuged in 50 mM HEPES buffer (pH of 8.0) at 10,000 rpm for 20 min at 4 °C. The pellets were resuspended in a 0.5% CTAC solution and then rehomogenized. MPO colorimetric assay was performed as previously described (Schierwagen et al. 1990) using 3,3′,5,5′-tetramethylbenzidine as the substrate for

$H_2O_2$ under low pH conditions. Results were expressed as MPO units per milligram of lung tissue.

### Cytokines in lung tissue and in the BAL fluid

A Bio-Plex Multiplex immunoassay from Bio-Rad (Mississauga, Ontario, Canada) was performed following the manufacturer's instruction on lung tissues and BAL fluid from control and ANP mice from experiment 1 for the following inflammatory mediators: IL-6, IL-10, keratinocyte-derived chemokine (KC), MCP-1, macrophage inflammatory protein (MIP)1α and MIP1β.

### Measurement of serum amylase activity and hematology

All mice were anesthetized with an intraperitoneal injection of a ketamine/xylazine mix (10:1) and blood collection was performed by an intracardiac puncture with a pre-heparinized syringe. Blood samples were kept on ice and were rapidly sent to the Prairie Diagnostic Services of the Western College of Veterinary Medicine for plasma amylase activity measurement and a hematology panel.

### Statistical analysis

Statistical analysis was performed using the statistical software GraphPad Prism 6 (GraphPad Software, La Jolla, CA, USA). Histological grading scores were expressed in medians with range and the comparison of medians was done by the nonparametric Kruskal-Wallis test followed by Dunn's multiple comparison test as post hoc test (experiment 1) or by the nonparametric Mann-Whitney test (experiment 2). Differences among plasma amylase activity means were detected by a one-way analysis of variance (ANOVA) on the ranked data followed by Tukey's multiple comparison test (experiment 1) or the nonparametric Kruskal-Wallis test followed by Dunn's multiple comparison test (experiment 2). CD68-labeling grid intersect ratios, lung MPO activity, BAL white blood cell counts and cytokine levels are expressed in means ± standard deviation (SD) and comparison of means among groups was done with one-way ANOVA followed by Tukey's multiple comparison test as post hoc test.

## Results

### Development of ANP in L-arginine–treated C57BL/6 mice

#### Pancreatic gross anatomy and histopathological grading

Gross pathological and histopathological changes were detectable in the pancreas of all mice that received L-arginine treatments whereas control mice had a normal anatomy and histology of the pancreas (total pancreatic histology score of 0) (Fig. 1a, b). At 24 h of the L-arginine treatment, the pancreas was edematous, enlarged and associated histologically with a multifocal mild loss of zymogen granules in acinar cells (Fig. 1c, d). Then, after 72 h, separation of pancreatic lobules along with a diffuse grayish discoloration was obvious macroscopically. Histological examination revealed diffuse necrosis in more than 50% of the pancreatic parenchyma, diffusely increased spaces between lobules, disruption of acinar cells, as well as massive infiltration of neutrophils in the pancreatic parenchyma (Fig. 1e, f). The pancreatic histopathological changes in the 72 h L-arginine group confirmed the development of ANP. Finally, 120 h following L-arginine treatments, the pancreas was markedly atrophic and only rare intact pancreatic acinar cells were distinguishable histologically due to extensive tissue damage and loss. Furthermore, at this stage, lymphocytes rather than neutrophils infiltrated the pancreatic parenchyma (Fig. 1g, h). The scores for each pancreatic histopathological grading category and the total pancreatic histopathology scores for each timepoint group are presented in Fig. (2a–d); the total pancreatic histopathology median score and range were as follows: for the 24 h L-arginine group, a median score of 1 and a range of 0–3; for the 72 h L-arginine group, a median score of 8 and a range of 6–10; and for the 120 h L-arginine group, a median score of 4 and a range of 2–10. The scores or pancreatic necrosis, pancreatic inflammatory cell infiltration and pancreatic histopathology were significantly increased at 72 h and 120 h post-arginine treatment while pancreatic edema was elevated at 72 h after the arginine injection.

### Plasma amylase activity

The mean values for the plasma amylase activity in each group of mice are as follows: control mice (1483 U/L ± 48 U/L), 24 h L-arginine group (5528 U/L ± 1210 U/L), 72 h L-arginine group (6547 U/L ± 1275 U/L) and 120 h L-arginine group (1399 U/L ± 62 U/L). Plasma amylase levels were significantly increased in the 24 h and 72 h groups of L-arginine–treated mice compared with the plasma amylase levels from the group of control mice ($p < 0.001$) (Fig. 2e). After 120 h, the plasma amylase of L-arginine–treated mice regained a basal level.

### Lung inflammation in ANP C57BL/6 mice

#### Lung histopathological grading

The lung histological evaluation (Fig. 3a–d) revealed an infiltration of mononuclear phagocytes in the alveolar septa of mice in the 72 h group only, which resulted in a total lung histopathology score significantly greater compared to that of

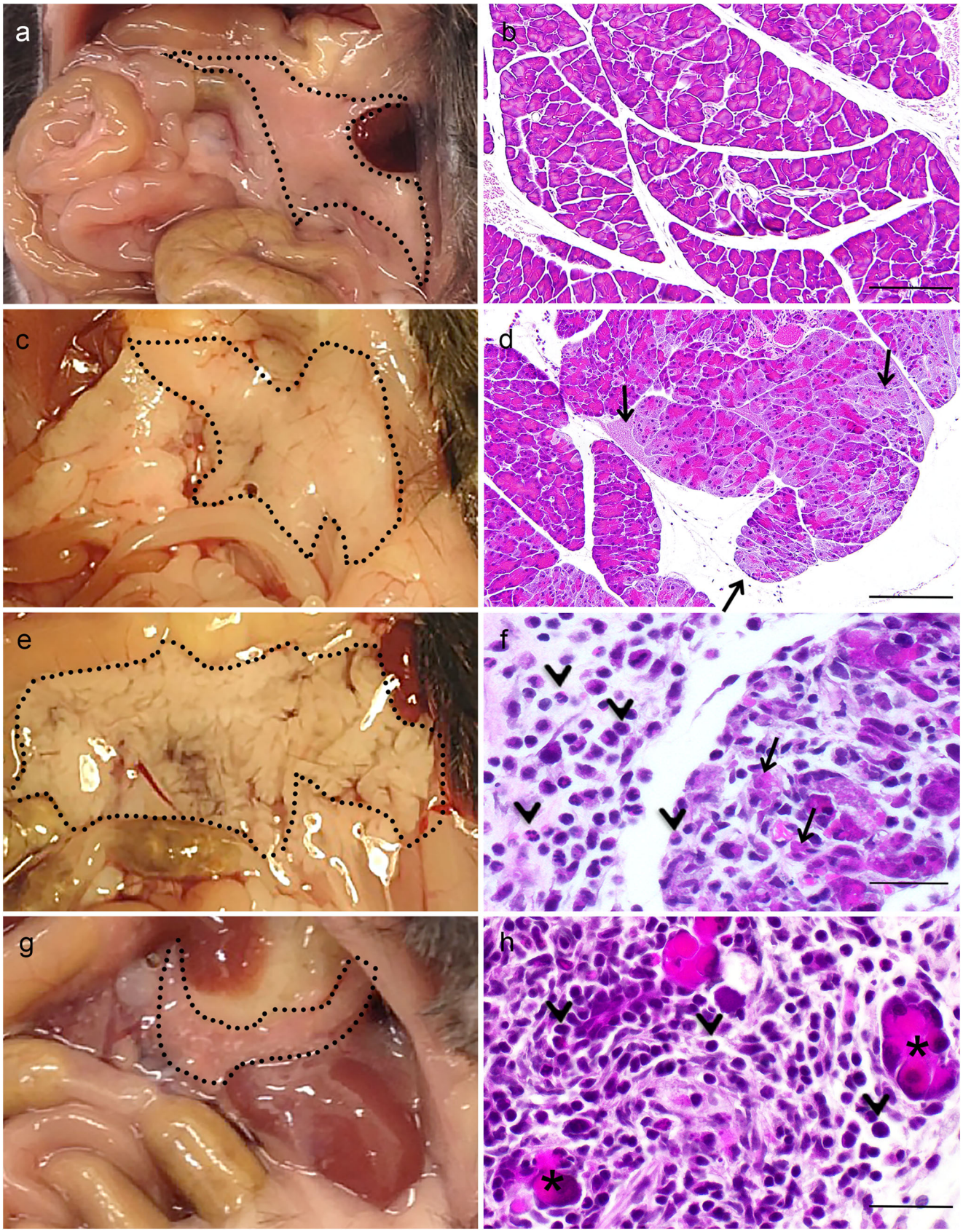
a
b
c
d
e
f
g
h

◀ **Fig. 1** Gross anatomy and histology (hematoxylin and eosin staining) of the pancreas of control and L-arginine–treated mice. Normal gross anatomy (**a**) and histology (**b**) of the pancreas of control mice. L-Arginine–treated mice after 24 h presented an enlarged and edematous pancreas (**c**), which is associated with a mild loss of zymogen granules in acinar cells (**d**; *arrows*). After 72 h, the pancreas of L-arginine–treated mice was discolored and gelatinous and had distended interlobular spaces (**e**) corresponding with acinar cell necrosis (**f**; *arrows*) and a marked infiltration of neutrophils in the pancreatic parenchyma and the interlobular spaces (**f**; *arrowheads*). After 120 h, the pancreas of L-arginine–treated mice was atrophic (**g**) and only scattered acinar cells remain (**h**; *stars*). At this stage, there was an abundant infiltration of mononuclear inflammatory cells (mainly lymphocytes) (**h**; *arrowheads*). The dotted lines delineate the pancreas. Scale bars in **b** and **d** are 200 μm and those in **f** and **h** are 60 μm

the control mice, which had scores of 0 in every grading category ($p < 0.001$) (Fig. 3e).

### CD68 immunohistochemistry

The negative and isotype controls resulted in the absence of immunolabeling. CD68 immunohistochemistry revealed a significant accumulation of macrophages in the pulmonary alveolar septa of mice at all of the timepoints after treatment with L-arginine compared to the control mice (Fig. 4a, b). The ratios of the total number of grid intersects overlaying CD68-positive septal macrophages to the total number of grid intersects overlaying alveolar septa were significantly greater in L-arginine–treated mice (24 h ratio mean, 0.0808 ± 0.0115; 72 h

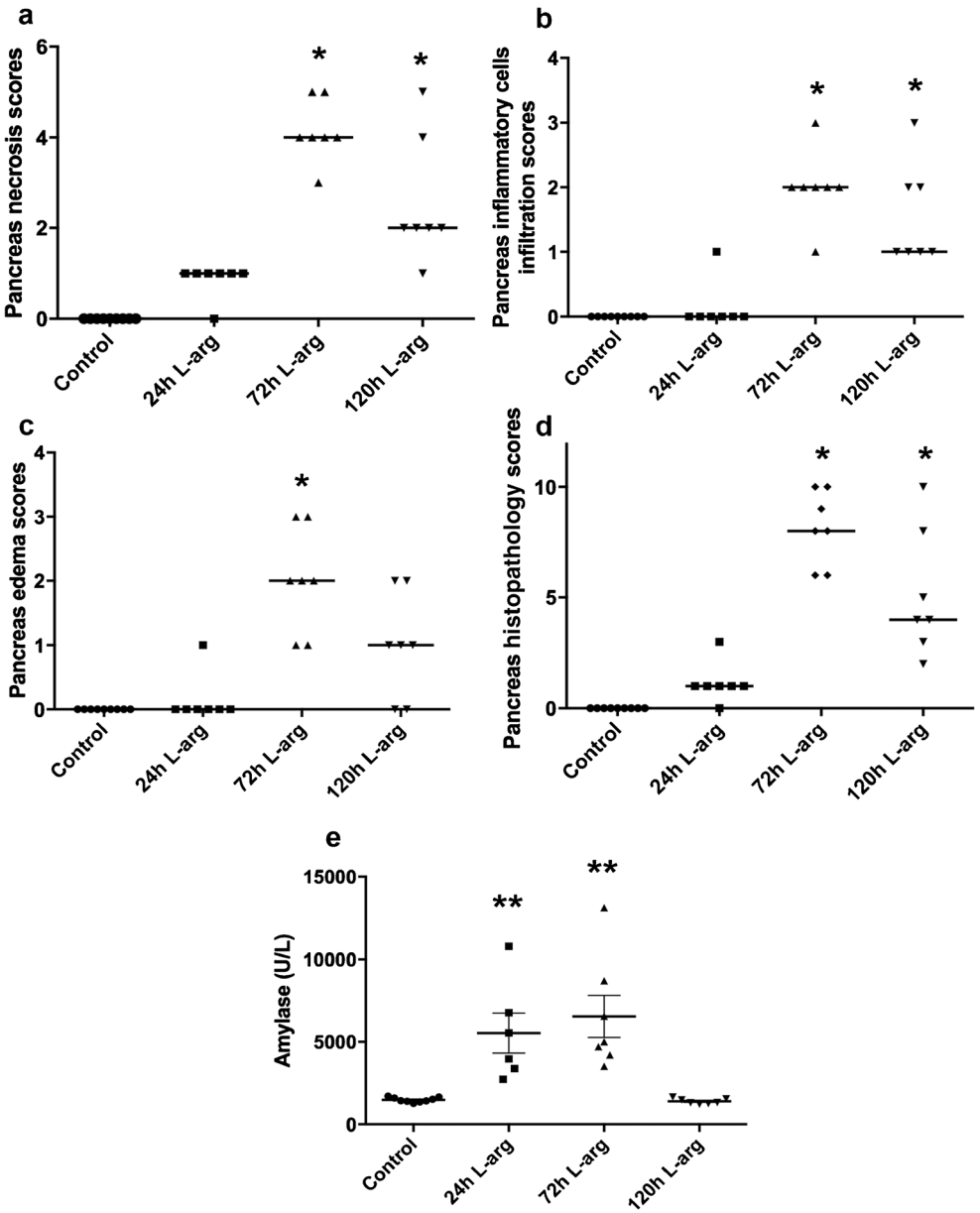


**Fig. 2** Pancreatic histological grading scores and plasma amylase levels from control and L-arginine–treated mice. **a** Pancreatic necrosis scores. **b** Inflammatory cell infiltrate scores. **c** Pancreatic edema scores. **d** Total histopathology scores (representing the sum of the three different scoring categories). **e** Plasma amylase levels. Median scores are represented by horizontal lines. Significant differences from control mice are denoted as follows: $*p < 0.0001$ and $**p < 0.001$; Kruskal-Wallis test followed by Dunn's multiple comparison test (**a**–**d**) and one-way ANOVA on the ranked data followed by Tukey's multiple comparison test (**e**)

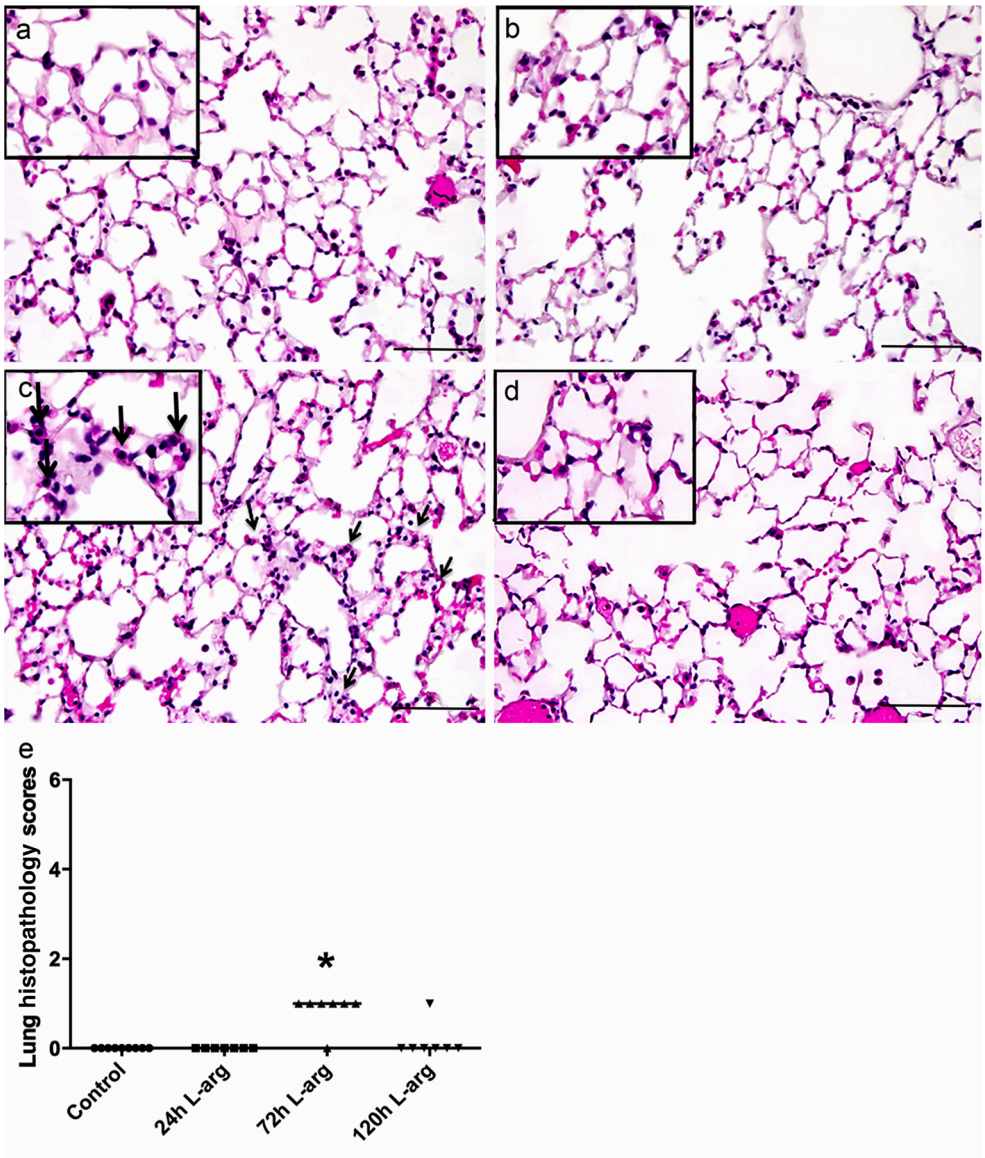


**Fig. 3** Lung histopathology (hematoxylin and eosin staining) of control mice (**a**) and L-arginine–treated mice after 24 h (**b**), after 72 h showing infiltrations of mononuclear inflammatory cells in alveolar septa (**c**; *arrows*) and after 120 h (**d**). Total lung histopathology scores (**e**). Score median values are represented by horizontal lines. Significant differences from control mice are denoted as follows: *$p < 0.001$; Kruskal-Wallis test followed by Dunn's multiple comparison test. All scale bars are 200 μm

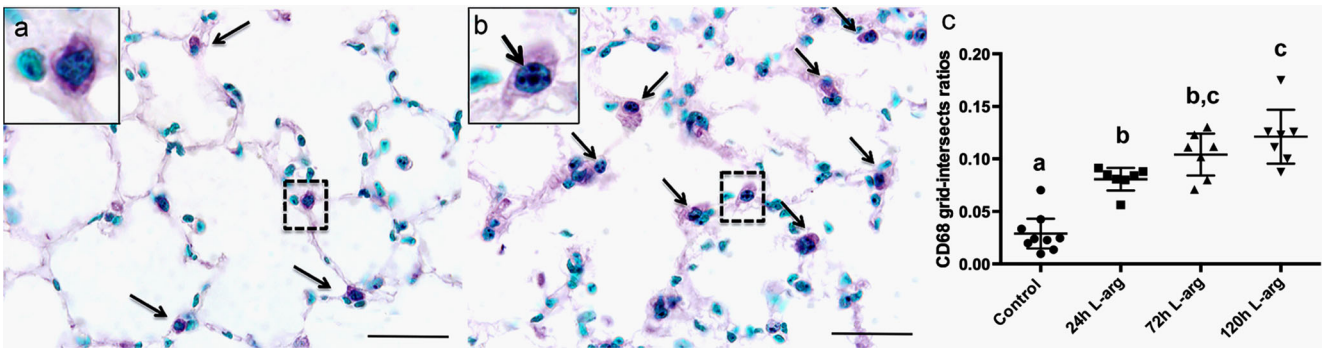


**Fig. 4** Immunohistochemistry against CD68 at 72 h. **a** Control mice showed rare CD68-positive macrophages in alveolar septa (*arrows*). **b** L-Arginine–treated mice had more numerous CD68-positive macrophages in alveolar septa (*arrows*). Inset: higher magnification showing intranuclear and intracytoplasmic CD68-positive staining in a septal macrophage of L-arginine–treated mice (**b**) compared to only intracytoplasmic CD68-positive staining in control mice (**a**). **c** Ratios of the number of grid intersects overlaying CD68-positive septal macrophages to the number of grid intersects overlaying alveolar septa in control mice compared to L-arginine–treated mice showing a gradual increase in septal macrophages in L-arginine–treated mice. Significant differences of $p < 0.0001$ are denoted by letters; one-way analysis of variance (ANOVA) followed by Tukey's multiple comparison test. All scale bars are 100 μm

ratio mean, 0.1041 ± 0.0217; 120 h ratio mean, 0.1212 ± 0.0278) compared to control mice (ratio mean, 0.0289 ± 0.0184; $p < 0.0001$) (Fig. 4c). Furthermore, the CD68 mean ratio from the 120 h L-arginine–treated group was significantly higher than the mean ratio from the 24 h L-arginine–treated group, suggesting that the recruitment of septal macrophages is sustained during the experimental period. Interestingly, it was noted in L-arginine–treated mice that the CD68 labeling was occasionally located in the nucleoplasm in addition to the cytoplasm, or only in the nucleoplasm, compared to control mice in which CD68 labeling was mainly observed in the cytoplasm (Fig. 4a, b). The intravascular presence of CD68 cells was confirmed with electron microscopy on lung tissues retrieved from paraffin-embedded tissue blocks (supplementary Figure 1).

### vWF immunohistochemistry

All L-arginine–treated mice and control mice presented vWF labeling of endothelial cells of larger blood vessels, including arteries, arterioles, venules and veins but not the airway epithelium (Fig. 5a). However, in mice with ANP, there was also granular labeling observed around large cells in the alveolar septal capillaries (Fig. 5b), a staining pattern rarely noticeable in control mice (Fig. 5a).

### Lung tissue and BAL cytokine levels

Lung tissue IL-6, IL-10 and MCP-1 protein concentrations were significantly increased compared to those of the control mice solely in the 24-h L-arginine–treated group from experiment 1 (Fig. 6a–c). However, there were no significant changes between groups for KC, MIP1α and MIP1β. The protein concentrations for all six aforementioned inflammatory mediators in the BAL fluid of L-arginine–treated mice were out of range or were not significantly different between the groups (data not shown).

### Total lung MPO activity

There were no differences in the total lung MPO activity (mean ± SD: control, 1.094 ± 0.2299; 24 h group, 1.208 ± 0.3691; 72 h group, 0.9469 ± 0.177; 120 h group, 0.8739 ± 0.1154; $p = 0.064$) among the groups. This suggests no differences in neutrophil recruitment.

### BAL fluid white blood cell counts and hematology

The total BAL WBC and macrophage counts did not show any differences among treatment groups (supplementary Figure 2). Furthermore, there were no statistical differences among the different treatment groups regarding the complete white blood cell counts and differential blood counts (data not shown).

## Development of ANP in L-arginine–treated MCP-1 KO mice

The pancreatic histology scores for control MCP-1 KO mice that received saline were 0 in every grading category. Based on the pancreatic histopathological grading and the plasma amylase activity level, one MCP-1 knockout mice treated with L-arginine did not develop ANP after 72 h; therefore, this mouse was excluded from the study. The other MCP-1 KO mice treated with L-arginine developed similar pancreatic lesions as for the C57BL/6 mice, including necrosis of the

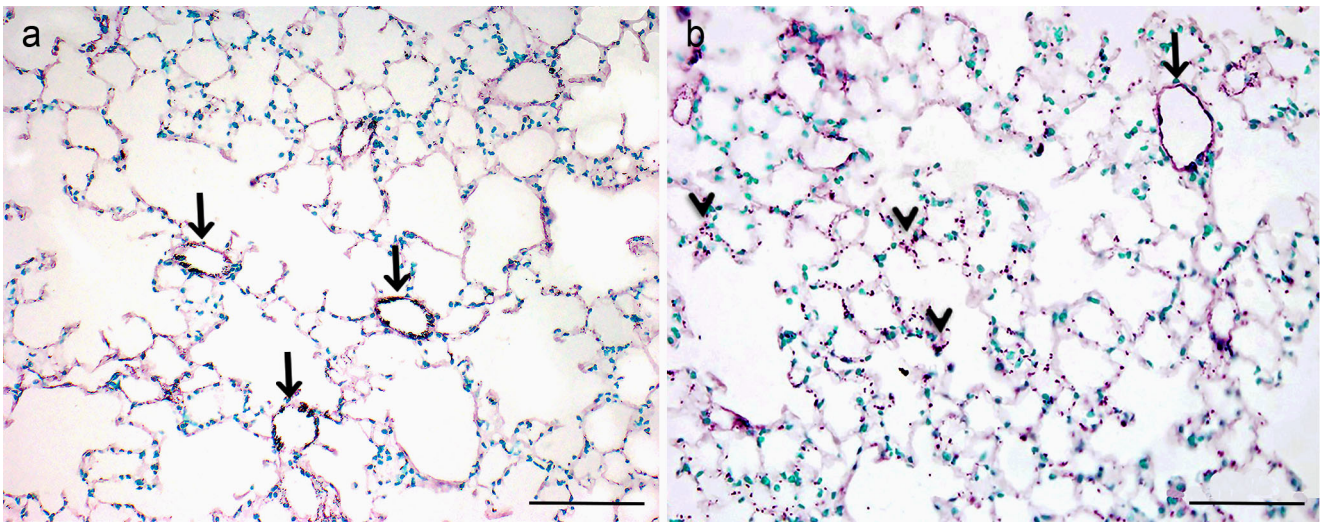


**Fig. 5** Immunohistochemistry against vWF. **a** In control mice, labeling for vWF was only present in endothelial cells of medium-large blood vessels (*arrows*). **b** In L-arginine–treated mice, labeling for vWF was present in alveolar septa (*arrowheads*) in addition to medium-large blood vessels (*arrow*). Inset: note the granular aspect of the staining in alveolar septal capillaries. All scale bars are 200 μm

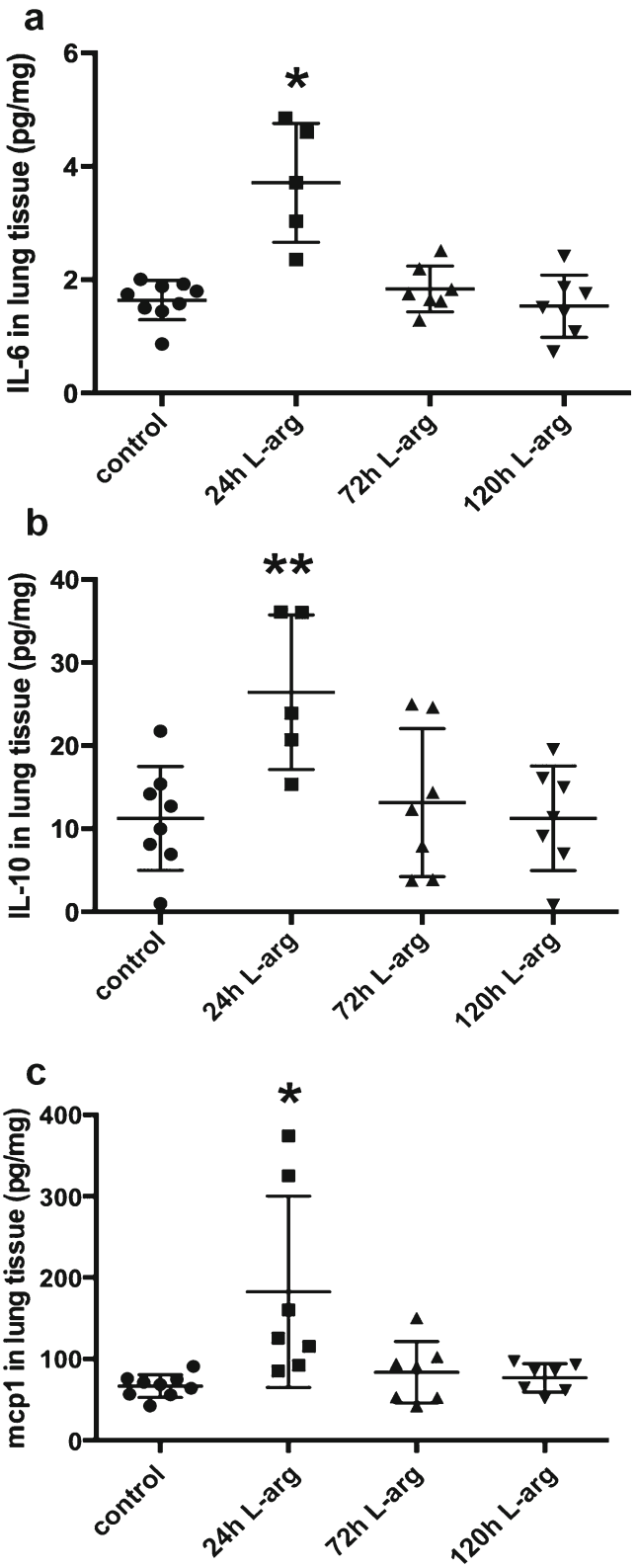


**Fig. 6** Lung tissue cytokine/chemokine levels in L-arginine–treated mice compared to control mice showing increased levels of IL-6 (**a**), IL-10 (**b**) and MCP-1 (**c**) in the 24 h L-arginine–treated mice. Significant differences from control mice are denoted as follows: $*p < 0.0001$ and $**p < 0.01$; one-way analysis of variance (ANOVA) followed by Tukey's multiple comparison test

pancreatic parenchyma (median score, 3.5; range, 1–5), infiltration of inflammatory cells (neutrophils) (median score, 1.5; range, 0–2) and pancreatic edema (median score, 1.5; range, 1–3). The total pancreatic histopathology score was similar between the L-arginine–treated C57BL/6 mice in the 72 h group (median, 8; range, 6–10) and in the L-arginine–treated MCP-1 KO group (median, 6; range, 3–10; $p = 0.5576$). Furthermore, the plasma amylase activity was similar between the L-arginine–treated C57BL/6 mice in the 72 h group (median, 5000 U/L; range, 3519–13,120) and in the L-arginine–treated MCP-1 KO group (median, 5756 U/L; range, 1535–11,955 U/L). The plasma amylase activity in the L-arginine–treated MCP1 KO group (median, 5756 U/L; range, 1535–11,955 U/L) was not statistically different compared to that in the MCP-1 KO control group (median, 1584 U/L; range, 1522–2203 U/L).

## Assessment of lung inflammation and PIM recruitment in ANP MCP-1 KO mice

### Lung histopathological grading

The lung histological evaluation revealed scores of 0 in every grading category for the MCP-1 KO control group and the L-arginine–treated MCP-1 KO group, except for one outlier that received a score of 1 (mild) in the inflammatory cell infiltrate category. Nevertheless, the total histology score was greater for L-arginine–treated C57BL/6 mice in the 72 h group (median, 1; range, 0–1) where the alveolar septum accumulation of mononuclear phagocytes was observed compared to MCP-1 KO mice (scores of 0, except for one outlier; $p < 0.05$) where the lung histology was mostly normal.

### CD68 immunohistochemistry

Based on the ratios of the total number of grid intersects overlaying CD68-positive septal macrophages to the total number of grid intersects overlaying alveolar septa, there was no significant difference in the number of macrophages present in the alveolar septa of L-arginine–treated MCP-1 KO mice (ratio mean, $0.03708 \pm 0.02064$) compared to control MCP-1 KO mice (ratio mean, $0.02378 \pm 0.01535$). Furthermore, the lungs of L-arginine–treated MCP-1 KO mice had lower numbers of induced PIMs compared to those of L-arginine–treated C57BL/6 mice in the 72 h group (ratio mean, $0.1041 \pm 0.0217$; $p < 0.0001$) (Fig. 7).

### vWF immunohistochemistry

vWF labeling was similar between the MCP-1 KO control mice and the MCP-1 KO mice treated with L-arginine; vWF labeling was only present in endothelial cells of larger blood

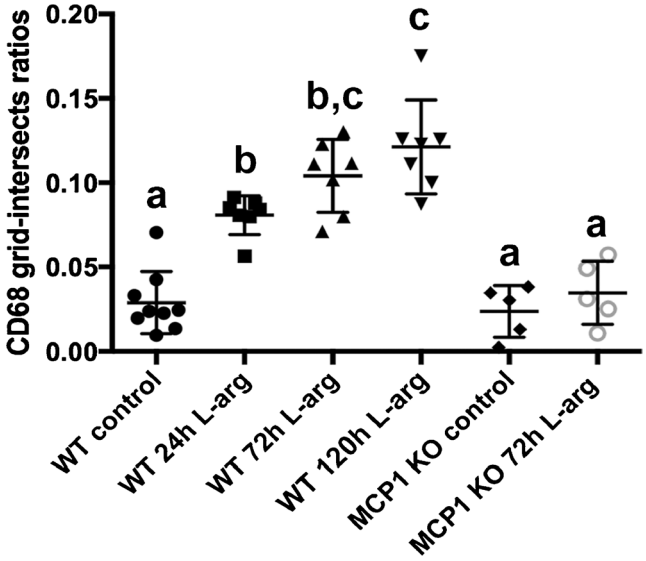


**Fig. 7** Ratios of the number of grid intersects overlaying CD68-positive septal macrophages to the number of grid intersects overlaying alveolar septa in control mice, L-arginine–treated WT mice and L-arginine–treated MCP-1 KO mice, at 72 h. Compared to WT mice with ANP at 72 h, septal macrophages, considered as induced PIMs, were not recruited in MCP-1 KO mice with ANP at 72 h. Significant differences of $p < 0.0001$ are denoted by letters; one-way analysis of variance (ANOVA) followed by Tukey's multiple comparison test

vessels, including arteries, arterioles, venules and veins (supplementary Figure 3).

## Discussion

Until now, studies on lung injury associated with severe AP in rodent models have mainly focused on the role of alveolar macrophages and, to a lesser extent, interstitial macrophages (Gea-Sorli et al. 2011). We have recently shown, using immunohistochemistry and electron microscopy, that PIMs are recruited in the lungs of dogs that died because of ANP (Vrolyk et al. 2016). Now, we report the first systematic assessment of recruitment of PIMs in a rodent model of ANP. The PIM recruitment was blocked by MCP-1–deficient PIM recruitment in L-arginine–treated mice. The data from these experiments set the stage for the use of a rodent model to study the intriguing role of induced PIMs in lung injury associated with ANP.

First, we used a well-established mouse model of ANP to establish that lung inflammation was obvious as early as 24 h following the L-arginine injections and persisted until the 120-h timepoint. The inflammation was assessed through histopathology, quantification of neutrophil recruitment and analyses of selected pro- and anti-inflammatory mediators. Increased lung levels of IL-6, MCP-1 and IL-10 were detected at 24 h following injection of L-arginine, which suggests an early lung inflammatory response. We recently demonstrated increased immunohistological staining for IL-6 in alveolar and recruited septal macrophages in the lungs of dogs that died of ANP (Vrolyk et al. 2016). Furthermore, in a rat model of severe AP, lung interstitial macrophages were attributed to a regulatory M2b phenotype characterized by the expression of the anti-inflammatory cytokine IL-10 (Gea-Sorli et al. 2011). However, considering the challenge of resolving the interstitium in the lung alveolar septum with a light microscope, it is likely that the macrophages identified as interstitial may be the intravascular macrophages. Although the multiplex assay on lung homogenates does not allow to identify the cell type responsible for the increased level of IL-10 in the lungs of ANP mice at 24 h in this study, interstitial macrophages may adopt an anti-inflammatory profile to temper the lung inflammatory response in the L-arginine model. The white blood cell counts and inflammatory cytokine levels in the BAL fluid were not significantly increased in the L-arginine–induced ANP mice compared to the control mice. During ANP, as the lungs are challenged through the vascular compartment, rather than the airways, the absence of significant changes in the cytokine levels and in the leukocyte population in the BAL fluid is not surprising. Interestingly, unlike what is reported in other studies that used the L-arginine–induced ANP model in mice to assess lung injury, the recruitment of neutrophils into the lungs of ANP mice in our study was not observed with histology and total lung MPO activity assay (Chen et al. 2012; Dawra et al. 2007). Although the reasons for this discrepancy are unclear, it could be due to factors such as differences in L-arginine doses administered and variable housing environment. It is also possible that the neutrophil recruitment was missed in the present study as only specific timepoints were examined. Nevertheless, it is notable that the evaluation of the lungs from naturally occurring ANP in dogs also showed a lack of neutrophil accumulation at the time of death (Vrolyk et al. 2016). This raises the suggestion that neutrophil recruitment is not a feature of lung inflammation associated with ANP or that it is an early transitory event that is easily missed.

The quantitation of labeling with anti-macrophage CD68 antibody demonstrated a significant increase of macrophages in the alveolar septa of the lungs of ANP mice compared with the control mice. In addition to the intratracheal instillation of fixative performed to obtain optimal lung morphology preservation, we used a well-established grid intersection counting system that controls for the potential lung volume variations among mice. We selected the CD68 antibody based on its common use for the identification of differentiated macrophages in the lungs of mice (Kim et al. 2008) and its reported use in identifying PIMs with immunohistochemistry in different species, including rats and cattle (Singh et al. 2004; Thenappan et al. 2011). Based on the grid intersect ratios, CD68-positive macrophages were significantly increased in the alveolar septa of the lungs of all mice with L-arginine–

induced ANP. Moreover, the results suggest that the recruitment of those septal macrophages occurs as soon as 24 h and is sustained until the 120-h timepoint, as shown by a significantly greater CD68-positive macrophage ratio mean at 120 h compared to the 24 h timepoint group. Although it is challenging with light microscopy to distinguish macrophages residing in the alveolar septal capillaries versus the interstitium, it is well recognized that the basement membranes of pulmonary capillary endothelial cells and alveolar epithelial cells are mostly fused. Thus, the interstitium does not provide the space required to contain large numbers of large cells, such as macrophages, which supports that most CD68-positive cells are located in the capillaries of alveolar septa and, therefore, are PIMs. Furthermore, as the CD68 antibody recognizes a lysosomal-associated membrane protein, positive staining in reactive macrophages is typically reported in the cytoplasm (Ackermann et al. 1994). Lastly, we used electron microscopy on lungs of dogs that died of ANP to show that the septal macrophages detected with an antibody were located in the lumen of pulmonary capillaries. Similarly, we have previously demonstrated in a rat model of bile duct ligation that recruited septal macrophages are indeed in the capillaries and, thus, are PIMs (Gill et al. 2008). Therefore, our data show PIM recruitment in a mouse model of ANP.

Having established that PIMs are recruited in this mouse model of ANP and that there is an increase in MCP-1, we used MCP-1 KO mice to determine the role of MCP-1 in PIM recruitment. Although ultrastructural studies in species with constitutive PIMs, such as in sheep and pigs, have demonstrated that PIMs originate from circulating monocytes that differentiate in mature macrophages within alveolar septal capillaries early after birth (Longworth et al. 1996; Winkler and Cheville 1987), the mechanisms of PIM recruitment are not fully understood. MCP-1 is a potent chemokine that attracts monocytes and macrophages to the site of inflammation in various conditions (Deshmane et al. 2009; Yadav et al. 2010). The lack of MCP-1 did not alter the development of ANP lesions in the MCP-1 KO mice based on pancreatic histopathological grading. One of the MCP-1 mice in this study did not develop ANP with L-arginine treatments because leakage of L-arginine solution from the abdominal injection site occurred immediately following one of the intraperitoneal injections. It has been reported that even a minor reduction of the L-arginine dose administered to mice can result in the complete absence of ANP development (Dawra et al. 2007). We do not know the reasons for the lack of statistical difference between the plasma amylase activity median in the L-arginine–treated MCP-1 KO mice and the control MCP-1 KO mice. Nevertheless, septal macrophage recruitment was significantly reduced in the lungs of MCP-1 KO mice with L-arginine–induced ANP compared with C57BL/6 mice with L-arginine–induced ANP. MCP-1 was previously suspected to be involved in the recruitment of PIMs in the lungs of rats with hepatopulmonary syndrome because these rats had increased lung levels of MCP-1 (Thenappan et al. 2011). Similar to our observations of increased MCP-1 in the lungs of mice with ANP, others have reported similar increases in lung MCP-1 levels in various pulmonary inflammatory conditions including endotoxin and lipoteichoic acid–induced lung injury, hepatopulmonary syndrome in rats and ARDS in human patients, during bacterial or influenza pneumonia, as well as in lung inflammation induced in other acute pancreatitis models than the L-arginine model (Dessing et al. 2007; Frossard et al. 2011; Rosseau et al. 2000; Thenappan et al. 2011; van Zoelen et al. 2011). Reported sources of MCP-1 in the lungs during inflammatory conditions include alveolar macrophages, type II pneumocytes and endothelial cells (Rosseau et al. 2000; Sanchez et al. 2007; Thorley et al. 2007). Furthermore, it is known that during vascular insults, activated endothelial cells secrete MCP-1, leading to the recruitment of monocytes (Niu and Kolattukudy 2009). After its release from endothelial cells, MCP-1 adheres to the vessel lumen and can participate in the arrest of the rolling monocytes on endothelial cells by binding the CCR2, found on the membrane of leukocytes, which could be involved in the initial steps of PIM recruitment (Niu and Kolattukudy 2009). During ANP, one possible source of MCP-1 in the lungs of affected animals could constitute the microvasculature endothelial cells. Indeed, the release of pancreatic digestive enzymes into the systemic circulation during ANP has been associated with microvascular injury in various remote organs, including the lungs (Pastor et al. 2003; Tahamont et al. 1982). In one study using MCP-1-deficient mice and a different model of acute pancreatitis (cerulein-induced pancreatitis), the infiltration of macrophages in the lungs as well as the severity of lung injury were reduced in the MCP-1 KO mice compared to the wild-type mice (Frossard et al. 2011). However, whether the improvement of lung injury in MCP-1 KO mice is mediated through the diminution/blockage of PIM induction remains to be further studied.

Our data show activation of lung microvascular endothelium in WT mice but not in MCP-1 KO mice injected with L-arginine. The endothelial activation was evidenced by the increased and granular immunolabeling for vWF at all timepoints in WT mice treated with L-arginine. A similar pattern of vWF staining was observed in the lungs of dogs that died due to ANP (Vrolyk et al. 2016). The granular vWF labeling pattern observed in alveolar septal capillaries (microvasculature) of mice with ANP was also reported in other species, including humans and dogs, with inflamed lungs or with lung vascular injury (Quan et al. 2009; Roberts et al. 2008). Furthermore, it has been reported that during vascular injury, endothelial cells from alveolar septal capillaries can synthesize and secrete vWF, which does not normally occur in quiescent alveolar septal endothelial cells and therefore, the presence of vWF labeling in the lung

microvasculature suggests vascular injury or activation (Mojiri et al. 2013). During acute pancreatitis, it is known that pancreatic proteases, including trypsin, elastase and phospholipase A2, are released into the blood circulation and can cause vascular injury to various organs, including the lungs (Pastor et al. 2003; Tahamont et al. 1982). As pancreatic enzymes are present in the blood circulation in the L-arginine mouse model, it is possible that those circulating enzymes stimulate endothelial cells of the lung microvasculature to synthesize and release vWF (Dawra et al. 2007). This staining could alternatively be platelets containing vWF as mouse platelets contain vWF in their α-granules (Kanaji et al. 2012). The role of vWF in lung inflammation associated with ANP in mice is not clear; however, it could promote leukocyte adhesion, including PIMs, as both vWF alone and vWF-platelet aggregation on endothelial cells were shown to promote rolling and adhesion of leukocytes to the endothelium at the site of inflammation (Bernardo et al. 2005; Pendu et al. 2006). It is possible that vWF and other molecules released by activated lung microvascular endothelium may also have contributed to PIM recruitment.

The development of L-arginine–induced ANP in this study resulted in similar pancreatic histological lesions and plasma amylase levels as in other studies using the same ANP mouse model with similar timepoints (Chen et al. 2012; Dawra et al. 2007; Shen et al. 2012a, b). It is noteworthy that after 120 h, the plasma amylase of L-arginine–treated mice regained a basal level, which is likely explained by the extensive depletion and destruction of pancreatic acinar cells and zymogen granules. Pancreatic lesions observed in the L-arginine–induced ANP mice in this study strongly resemble pancreatic lesions described in clinical cases of dog (Mansfield et al. 2012; Newman et al. 2006; Vrolyk et al. 2016) and human patients (Aho et al. 1982; Kloppel et al. 1986) suffering from this condition. Both human beings and dogs suffering from severe AP can present pulmonary complications and they both lack constitutive PIMs.

PIMs are now established as pro-inflammatory regulators of lung inflammation in species where they are constitutively present, as well as those in which they are induced during pathological conditions (Gill et al. 2008; Schneberger et al. 2009; Singh et al. 2004). During sepsis and endotoxemia, pro-inflammatory signaling pathways in PIMs are suggested to occur through TLRs, such as TLR4, TLR9 and TLR2 and following their activation, PIMs potentially produce large amounts of pro-inflammatory mediators such as TNF-α and IL-1β (Gill et al. 2008; Schneberger et al. 2009; Singh et al. 2004; Singh Suri et al. 2006). Based on our understanding that PIMs exacerbate lung inflammation following microbial challenges, their recruitment in the lungs of veterinary or human patients with ANP could have significant detrimental consequences if those patients secondarily develop endotoxemia or septicemia, as sometimes reported during the course of this disease (Ammori 2003).

## Conclusion

Because of the frequently reported respiratory complications in human or dog patients suffering from severe AP and the recent discovery that PIMs are recruited in dogs with clinical ANP, we sought to determine the recruitment of PIMs in a mouse model of severe AP. The results from this study not only bring evidence that PIMS are recruited in mice with L-arginine–induced ANP but also suggest that MCP-1 is involved in the recruitment mechanisms of those pulmonary macrophages. In addition, the data show significantly increased expression of vWF and inflammatory mediators, such as IL-6 and IL-10, in the lungs of mice with L-arginine–induced ANP. The induction of PIMs during ANP may increase the susceptibility of the lungs to develop an exacerbated lung inflammatory response in affected patients.

**Funding information** The research project was supported through a Discovery Grant from the Natural Sciences and Engineering Research Council of Canada. Dr. Vrolyk was supported by an Interprovincial Graduate Scholarship from the Western College of Veterinary Medicine, University of Saskatchewan.

## Compliance with ethical standards

**Conflict of interest** The authors declare that they have no conflict of interest.

**Ethical approval** All procedures performed in studies involving animals were in accordance with the ethical standards of the institution or practice at which the studies were conducted.

## References

Ackermann MR, DeBey BM, Stabel TJ, Gold JH, Register KB, Meehan JT (1994) Distribution of anti-CD68 (EBM11) immunoreactivity in formalin-fixed, paraffin-embedded bovine tissues. Vet Pathol 31: 340–348

Aharonson-Raz K, Singh B (2010) Pulmonary intravascular macrophages and endotoxin-induced pulmonary pathophysiology in horses. Can J Vet Res 74:45–49

Aho HJ, Nevalainen TJ, Havia VT, Heinonen RJ, Aho AJ (1982) Human acute pancreatitis: a light and electron microscopic study. Acta Pathol Microbiol Immunol Scand A 90:367–373

Ammori BJ (2003) Role of the gut in the course of severe acute pancreatitis. Pancreas 26:122–129

Atwal OS, Singh B, Staempfli H, Minhas K (1992) Presence of pulmonary intravascular macrophages in the equine lung: some structuro-functional properties. Anat Rec 234:530–540

Bernardo A, Ball C, Nolasco L, Choi H, Moake JL, Dong JF (2005) Platelets adhered to endothelial cell-bound ultra-large von Willebrand factor strings support leukocyte tethering and rolling under high shear stress. J Thromb Haemost 3:562–570

Brain JD, Molina RM, DeCamp MM, Warner AE (1999) Pulmonary intravascular macrophages: their contribution to the mononuclear phagocyte system in 13 species. Am J Phys 276:L146–L154

Chen J, Cai QP, Shen PJ, Yan RL, Wang CM, Yang DJ, Fu HB, Chen XY (2012) Netrin-1 protects against L-arginine-induced acute pancreatitis in mice. PLoS One 7:e46201

Dawra R, Sharif R, Phillips P, Dudeja V, Dhaulakhandi D, Saluja AK (2007) Development of a new mouse model of acute pancreatitis induced by administration of L-arginine. Am J Physiol Gastrointest Liver Physiol 292:G1009–G1018

Dehring DJ, Wismar BL (1989) Intravascular macrophages in pulmonary capillaries of humans. Am Rev Respir Dis 139:1027–1029

Deshmane SL, Kremlev S, Amini S, Sawaya BE (2009) Monocyte chemoattractant protein-1 (MCP-1): an overview. J Interf Cytokine Res 29:313–326

Dessing MC, van der Sluijs KF, Florquin S, van der Poll T (2007) Monocyte chemoattractant protein 1 contributes to an adequate immune response in influenza pneumonia. Clin Immunol 125:328–336

Frossard JL, Lenglet S, Montecucco F, Steffens S, Galan K, Pelli G, Spahr L, Mach F, Hadengue A (2011) Role of CCL-2, CCR-2 and CCR-4 in cerulein-induced acute pancreatitis and pancreatitis-associated lung injury. J Clin Pathol 64:387–393

Gea-Sorli S, Guillamat R, Serrano-Mollar A, Closa D (2011) Activation of lung macrophage subpopulations in experimental acute pancreatitis. J Pathol 223:417–424

Gill SS, Suri SS, Janardhan KS, Caldwell S, Duke T, Singh B (2008) Role of pulmonary intravascular macrophages in endotoxin-induced lung inflammation and mortality in a rat model. Respir Res 9:69

Hoyos S, Granell S, Heredia N, Bulbena O, Closa D, Fernandez-Cruz L (2005) Influence of portal blood on the development of systemic inflammation associated with experimental acute pancreatitis. Surgery 137:186–191

Kanaji S, Fahs SA, Shi Q, Haberichter SL, Montgomery RR (2012) Contribution of platelet vs. endothelial VWF to platelet adhesion and hemostasis. J Thromb Haemost 10:1646–1652

Kawashima M, Kuwamura M, Takeya M, Yamate J (2004) Morphologic characteristics of pulmonary macrophages in cetaceans: particular reference to pulmonary intravascular macrophages as a newly identified type. Vet Pathol 41:682–686

Kim EY, Battaile JT, Patel AC, You Y, Agapov E, Grayson MH, Benoit LA, Byers DE, Alevy Y, Tucker J, Swanson S, Tidwell R, Tyner JW, Morton JD, Castro M, Polineni D, Patterson GA, Schwendener RA, Allard JD, Peltz G, Holtzman MJ (2008) Persistent activation of an innate immune response translates respiratory viral infection into chronic lung disease. Nat Med 14:633–640

Klingensmith WC 3rd, Ryerson TW (1973) Lung uptake of 99m Tc-sulfur colloid. J Nucl Med 14:201–204

Kloppel G, Dreyer T, Willemer S, Kern HF, Adler G (1986) Human acute pancreatitis: its pathogenesis in the light of immunocytochemical and ultrastructural findings in acinar cells. Virchows Arch A Pathol Anat Histopathol 409:791–803

Longworth KE, Albertine KH, Staub NC (1996) Ultrastructural quantification of pulmonary intravascular macrophages in newborn and 2-week-old lambs. Anat Rec 246:238–244

Mansfield CS, Anderson GA, O'Hara AJ (2012) Association between canine pancreatic-specific lipase and histologic exocrine pancreatic inflammation in dogs: assessing specificity. J Vet Diagn Investig 24: 312–318

Mikami Y, Takeda K, Shibuya K, Qiu-Feng H, Egawa S, Sunamura M, Matsuno S (2002) Peritoneal inflammatory cells in acute pancreatitis: relationship of infiltration dynamics and cytokine production with severity of illness. Surgery 132:86–92

Mojiri A, Nakhaii-Nejad M, Phan WL, Kulak S, Radziwon-Balicka A, Jurasz P, Michelakis E, Jahroudi N (2013) Hypoxia results in upregulation and de novo activation of von Willebrand factor expression in lung endothelial cells. Arterioscler Thromb Vasc Biol 33:1329–1338

Molina RM, Brain JD (2007) In vivo comparison of cat alveolar and pulmonary intravascular macrophages: phagocytosis, particle clearance, and cytoplasmic motility. Exp Lung Res 33:53–70

Newman SJ, Steiner JM, Woosley K, Williams DA, Barton L (2006) Histologic assessment and grading of the exocrine pancreas in the dog. J Vet Diagn Investig 18:115–118

Niu J, Kolattukudy PE (2009) Role of MCP-1 in cardiovascular disease: molecular mechanisms and clinical implications. Clin Sci (Lond) 117:95–109

Pastor CM, Matthay MA, Frossard JL (2003) Pancreatitis-associated acute lung injury: new insights. Chest 124:2341–2351

Pendu R, Terraube V, Christophe OD, Gahmberg CG, de Groot PG, Lenting PJ, Denis CV (2006) P-selectin glycoprotein ligand 1 and beta2-integrins cooperate in the adhesion of leukocytes to von Willebrand factor. Blood 108:3746–3752

Pintado MC, Trascasa M, Arenillas C, de Zarate YO, Pardo A, Blandino A, de Pablo R (2016) New Atlanta classification of acute pancreatitis in intensive care unit: complications and prognosis. Eur J Intern Med 30:82–87

Quan L, Ishikawa T, Zhao D, Michiue T, Yoshida C, Chen JH, Wang Q, Zhu BL, Maeda H (2009) Immunohistochemistry of von Willebrand factor in the lungs with regard to the cause of death in forensic autopsy. Leg Med (Tokyo) 11(Suppl 1):S294–S296

Roberts GT, Ghebeh H, Chishti MA, Al-Mohanna F, El-Sayed R, Al-Mohanna F, Bouchama A (2008) Microvascular injury, thrombosis, inflammation, and apoptosis in the pathogenesis of heatstroke: a study in baboon model. Arterioscler Thromb Vasc Biol 28:1130–1136

Rosseau S, Hammerl P, Maus U, Walmrath HD, Schutte H, Grimminger F, Seeger W, Lohmeyer J (2000) Phenotypic characterization of alveolar monocyte recruitment in acute respiratory distress syndrome. Am J Physiol Lung Cell Mol Physiol 279:L25–L35

Sanchez O, Marcos E, Perros F, Fadel E, Tu L, Humbert M, Dartevelle P, Simonneau G, Adnot S, Eddahibi S (2007) Role of endothelium-derived CC chemokine ligand 2 in idiopathic pulmonary arterial hypertension. Am J Respir Crit Care Med 176:1041–1047

Schierwagen C, Bylund-Fellenius AC, Lundberg C (1990) Improved method for quantification of tissue PMN accumulation measured by myeloperoxidase activity. J Pharmacol Methods 23:179–186

Schneberger D, Caldwell S, Suri SS, Singh B (2009) Expression of toll-like receptor 9 in horse lungs. Anat Rec 292:1068–1077

Schneberger D, Lewis D, Caldwell S, Singh B (2011) Expression of toll-like receptor 9 in lungs of pigs, dogs and cattle. Int J Exp Pathol 92: 1–7

Shen J, Wan R, Hu G, Wang F, Shen J, Wang X (2012a) Involvement of thrombopoietin in acinar cell necrosis in L-arginine-induced acute pancreatitis in mice. Cytokine 60:294–301

Shen J, Wan R, Shen Z, Gao J, Wang X, Qian L, Lu H, Han W, Wang X (2012b) Chemokine receptor CXCR3 is involved in the acute pancreatitis-associated lung injury. Biomed Pharmacother 66:390–396

Shih WJ, Domstad PA, Friedman B, DeLand FH (1986) Intrathoracic abnormalities demonstrated by technetium-99m sulfur colloid imaging. Clin Nucl Med 11:792–796

Singh Suri S, Janardhan KS, Parbhakar O, Caldwell S, Appleyard G, Singh B (2006) Expression of toll-like receptor 4 and 2 in horse lungs. Vet Res 37:541–551

Singh B, Doane KJ, Niehaus GD (1998) Ultrastructural and cytochemical evaluation of sepsis-induced changes in the rat pulmonary intravascular mononuclear phagocytes. J Anat 192(Pt 1):13–23

Singh B, Pearce JW, Gamage LN, Janardhan K, Caldwell S (2004) Depletion of pulmonary intravascular macrophages inhibits acute lung inflammation. Am J Physiol Lung Cell Mol Physiol 286: L363–L372

Spanier B, Bruno MJ, Dijkgraaf MG (2013) Incidence and mortality of acute and chronic pancreatitis in the Netherlands: a nationwide

record-linked cohort study for the years 1995-2005. World J Gastroenterol 19:3018–3026

Tahamont MV, Barie PS, Blumenstock FA, Hussain MH, Malik AB (1982) Increased lung vascular permeability after pancreatitis and trypsin infusion. Am J Pathol 109:15–26

Thenappan T, Goel A, Marsboom G, Fang YH, Toth PT, Zhang HJ, Kajimoto H, Hong Z, Paul J, Wietholt C, Pogoriler J, Piao L, Rehman J, Archer SL (2011) A central role for CD68(+) macrophages in hepatopulmonary syndrome. Reversal by macrophage depletion. Am J Respir Crit Care Med 183:1080–1091

Thorley AJ, Ford PA, Giembycz MA, Goldstraw P, Young A, Tetley TD (2007) Differential regulation of cytokine release and leukocyte migration by lipopolysaccharide-stimulated primary human lung alveolar type II epithelial cells and macrophages. J Immunol 178:463–473

Tsukahara Y, Morisaki T, Horita Y, Torisu M, Tanaka M (1999) Phospholipase A2 mediates nitric oxide production by alveolar macrophages and acute lung injury in pancreatitis. Ann Surg 229:385–392

van Zoelen MA, Verstege MI, Draing C, de Beer R, van't Veer C, Florquin S, Bresser P, van der Zee JS, te Velde AA, von Aulock S, van der Poll T (2011) Endogenous MCP-1 promotes lung inflammation induced by LPS and LTA. Mol Immunol 48:1468–1476

Vrolyk V, Wobeser BK, Al-Dissi AN, Carr A, Singh B (2017) Lung inflammation associated with clinical acute necrotizing pancreatitis in dogs. Vet Pathol 54:129–140

Warner AE, Barry BE, Brain JD (1986) Pulmonary intravascular macrophages in sheep. Morphology and function of a novel constituent of the mononuclear phagocyte system. Lab Investig 55:276–288

Winkler GC, Cheville NF (1987) Postnatal colonization of porcine lung capillaries by intravascular macrophages: an ultrastructural, morphometric analysis. Microvasc Res 33:224–232

Yadav A, Saini V, Arora S (2010) MCP-1: chemoattractant with a role beyond immunity: a review. Clin Chim Acta 411:1570–1579

Zhao X, Jin B, Yang B, Yan W, Wu X, Jiang C, Cheng S (2017) Gadolinium chloride ameliorates acute lung injury associated with severe acute pancreatitis in rats by regulating CYLD/NF-kappaB signaling. Biochem Biophys Res Commun 492:255–261